

## Article

# A True Non-Newtonian Electrolyte for Rechargeable Hybrid Aqueous Battery

Tuan K. A. Hoang <sup>1</sup>, Longyan Li <sup>1,2</sup>, Jian Zhi <sup>1</sup>, The Nam Long Doan <sup>1</sup>, Wenhan Dong <sup>1</sup>, Xiaoxiao Huang <sup>1,3</sup>, Junhong Ma <sup>1,4</sup>, Yahong Xie <sup>1,4</sup>, Menglei Chang <sup>1,5</sup> and P. Chen <sup>1,\*</sup>

- <sup>1</sup> Department of Chemical Engineering and Waterloo Institute for Nanotechnology, University of Waterloo, 200 University Avenue West, Waterloo, ON N2L3G1, Canada; hoangk@uwaterloo.ca (T.K.A.H.); lilongyan@nuist.edu.cn (L.L.); z4jian@uwaterloo.ca (J.Z.); t6doan@uwaterloo.ca (T.N.L.D.); w5dong@uwaterloo.ca (W.D.); swliza@hit.edu.cn (X.H.); junhong@xju.edu.cn (J.M.); xyh0707@163.com (Y.X.); mengleic@sina.com (M.C.)
- <sup>2</sup> School of Chemistry and Materials Science, Nanjing University of Information Science and Technology, Nanjing 210044, China
- <sup>3</sup> School of Materials Science and Engineering, Harbin Institute of Technology, Harbin 150001, China
- <sup>4</sup> College of Chemical Engineering, Xinjiang University, Urumqi 830046, China
- <sup>5</sup> School of Materials Science and Energy Engineering, Foshan University, Foshan 528000, China
- \* Correspondence: p4chen@uwaterloo.ca; Tel.: +1-519-888-4567 (ext. 35586); Fax: +1-519-888-4347

**Abstract:** The rechargeable aqueous hybrid battery is a unique system in which the Li-ion mechanism dominates the cathode while the first-order metal reaction of stripping/depositing regulates the anode. This battery inherits the advantages of the low-cost anode while possessing the capability of the Li-ion cathode. One of the major challenges is to design a proper electrolyte to nourish such strengths and alleviate the downsides, because two different mechanisms are functioning separately at the node–electrolyte and the cathode–electrolyte interfaces. In this work, we design a non-Newtonian electrolyte which offers many advantages for a Zn/LiMn<sub>2</sub>O<sub>4</sub> battery. The corrosion is kept low while almost non-dendritic zinc deposition is confirmed by chronoamperometry and ex situ microscopy. The gel strength and gelling duration of such non-Newtonian electrolytes can be controlled. The ionic conductivity of such gels can reach 60 mS·cm<sup>-1</sup>. The battery exhibits reduced self-discharge, 6–10% higher specific discharge capacity than the aqueous reference battery, high rate capability, nearly 80% capacity retention after 1000 cycles, and about 100 mAh·g<sup>-1</sup> of specific discharge capacity at cycle No. 1000th. Negligible amorphization on the cathode surface and no passivation on the anode surface are observed after 1000 cycles, evidenced by X-ray diffraction and scanning electron microscopy on the post-run battery electrodes.



**Citation:** Hoang, T.K.A.; Li, L.; Zhi, J.; Doan, T.N.L.; Dong, W.; Huang, X.; Ma, J.; Xie, Y.; Chang, M.; Chen, P. A True Non-Newtonian Electrolyte for Rechargeable Hybrid Aqueous Battery. *Batteries* **2022**, *8*, 71. <https://doi.org/10.3390/batteries8070071>

Academic Editor: Carlos Zieber

Received: 26 May 2022

Accepted: 7 July 2022

Published: 13 July 2022

**Publisher's Note:** MDPI stays neutral with regard to jurisdictional claims in published maps and institutional affiliations.



**Copyright:** © 2022 by the authors. Licensee MDPI, Basel, Switzerland. This article is an open access article distributed under the terms and conditions of the Creative Commons Attribution (CC BY) license (<https://creativecommons.org/licenses/by/4.0/>).

## 1. Introduction

Zinc batteries had been studied for a few decades before the lithium-ion batteries gained interest [1–5]. While Li-ion batteries have been widely commercialised, only the primary Zn/MnO<sub>2</sub> battery is widely available [6–10]. Li-ion technologies are now available in small devices, such as cell phones, to large devices, such as electric cars and trucks. Zinc-based batteries mainly come in small sizes, for use in small tools and instruments. Scaling up zinc batteries is more difficult. The major limitation of zinc batteries is at the zinc anode, which is not very stable in an aqueous environment (both mild acidic and alkaline) [11–15]. Major problems include passivation, corrosion, and dendrite formation [16]. The passivation process consists of the deposits of non-soluble Zn<sup>2+</sup> oxide or hydroxide salts on the zinc anode. These deposits are more insulating, and they break the conductive continuum between the anode and the electrolyte. On the other hand, the corrosion is related to the irreversible dissolution of the Zn anode into the electrolyte and the electrolysis of water,

which leads to the revolution of hydrogen gas bubbles and the unwanted increases in  $Zn^{2+}$  concentration in the electrolyte [17]. Both passivation and corrosion increase the internal resistance as well as the polarisation of the battery. Thus, both phenomena are detrimental to the energy storage efficiency and deteriorate the electrochemical performance of the battery [18]. Its lifetime could be significantly reduced.

The dendrite formation on the anode is a critical issue that jeopardises zinc batteries. This problem is not just observed in zinc batteries, but it is also a widely acknowledged issue among lithium batteries [19]. As is widely recognised, the dendrite formation is basically attributed to the roughness of the anode surface, which results in the uneven distribution of the electric charges. During the discharge process,  $Zn^{2+}$  ions are released from the anode due to the oxidation of metal zinc, whereas in the charge process,  $Zn^{2+}$  ions are reduced and prone to deposit on the sites with defects or higher ionic conductivity. This deposition behaviour leads to the non-homogeneous distribution of both the zinc atoms and the stress on the anode surface. Thus, the non-uniform dendritic structures may grow in the form of extrusions, which pierce through the separator, reach the cathode, and cause a short circuit [20]. Due to this freestyle growth of the dendrites, the electrochemical performance such as the energy density and the cycle life of the batteries degenerates rapidly after certain periods of time, and even safety issues will arise. Therefore, it is important to minimise the dendrite formation on the zinc surface. For this purpose, research works concerning the development of new forms of anodes and new electrolytes have been being continuously developed [21,22].

In this paper, we describe our design on a new non-Newtonian electrolyte for the secondary aqueous  $Zn/LiMn_2O_4$  battery. The electrolyte is thixotropic due to the existence of fumed silica (FS) as one of the gelling agents. Thixotropy is an important property in that it allows one to “liquefy” the gel electrolyte by applying appropriate shear stress, which is conducive to introducing the electrolyte into the separator before it totally transforms into the solid state after a certain duration of time [23,24]. This thixotropic property renders the electrolytes non-Newtonian materials. In this work, polyvinyl alcohol (PVA), a non-thixotropic gelling agent, is adopted to adjust the gelling duration of the electrolyte by cooperating with the fumed silica (a thixotropic gelling agent). The obtained gels are still thixotropic, but with different gelling periods. Furthermore, the PVA mitigates corrosion on the anode, which liberates us from adding an additional corrosion inhibitor (e.g., inorganic  $Pb^{2+}$  or organic pyrazole) into the electrolyte. This is the first time that this gel system is formulated and applied in the rechargeable hybrid aqueous battery. As a result, the corrosion current density of the PVA-containing gel electrolytes is lower than the corrosion exerted by non-PVA gel electrolytes, the dendrite formation on the  $Zn$  anode is suppressed, and the cyclability of the gelled batteries is improved. To be specific, after 1000 cycles, the PVA-FS gelled battery reaches 78% of capacity retention, while only 63% is observed on the reference aqueous battery. Furthermore, the specific discharge capacity of PVA-containing gelled batteries is higher. After 1000 cycles, the battery still can offer about  $100 \text{ mAh}\cdot\text{g}^{-1}$ . Amorphization on the cathode surface is suppressed and passivation on the zinc anode is reduced thanks to the ex-situ crystallography and microscopy results on the post-run battery electrodes.

## 2. Experimental Section

### 2.1. Preparation of Batteries

The cathode and the anode were prepared as described in our previous report [25]. The typical active material load of the cathode was  $3\text{--}6 \text{ mg}\cdot\text{cm}^{-2}$ .

Preparation of the electrolyte: The preparation was conducted on the bench and in the fume hood, using a stirring machine, at room conditions. The electrolytes were prepared using 130.57 g of  $\text{Li}_2\text{SO}_4\cdot\text{H}_2\text{O}$  (Sigma Aldrich, St. Louis, MO, USA, 98%) and 146.20 g of  $\text{ZnSO}_4\cdot7\text{H}_2\text{O}$  (Sigma Aldrich, 98%) in deionised water and adjusted to 500 mL. It contains 2M  $\text{Li}_2\text{SO}_4$  and 1M  $\text{ZnSO}_4$ . The pH was adjusted to  $4.00 \pm 0.05$  by introducing a few drops of concentrated LiOH aqueous solution into the aqueous electrolyte under stirring at

room temperature. The electrolyte is named (#33) and batteries containing this electrolyte are named the (#33). Gel electrolytes of 5% FS, 4% FS + 1% PVA, and 3% FS + 2% PVA were prepared by mixing conventional liquid electrolyte with as-received fumed silica (Sigma Aldrich) and polyvinyl alcohol (99%, Sigma Aldrich) under vigorous stirring at room condition. During stirring, the electrolyte vial was always capped to avoid water evaporation. Batteries with such electrolytes will be labelled as “the 5% FS”, “4% FS + 1% PVA” and “3% FS + 2% PVA”, respectively.

## 2.2. Instrumentation

Gel strength was studied via the ball penetration experiment [24,26,27]. Fresh cathode and anode, post-battery-run cathodes, and anodes were examined via diffraction and field emission scanning electron microscopy. Functional groups of PVA, fumed silica, and gel electrolytes were analysed via Fourier transform infrared spectroscopy at room condition (FT-IR, Brüker Vector 70), using an attenuated total reflectance (ATR) sample stage.

## 2.3. Electrochemical Measurements

The conductivity, chronoamperometry, corrosion, and battery testing procedures were the same as those reported in the literature [25]. All electrochemical data were obtained at about 20 °C (room condition).

## 3. Results and Discussion

In Table 1, it was reported that the ball penetration depth is 7.3–8.1 mm. If the ball is going through the gel, the gel is considered too soft. Otherwise, no penetration means the gel is too hard. This testing method was adapted from studies on the gel strength of thixotropic gel electrolytes. A decent penetration means that the gel strength is at the same magnitude with gels in VRLA batteries, which use the same AGM separators. Hard gels cannot fill the void space of the AGM separator effectively. Soft gels have too long a gelling time and slow down the manufacturing process unnecessarily [26,27].

**Table 1.** Physical characteristics of the PVA-FS gel system.

Gel Types	5% FS	4% FS + 1% PVA	3% FS + 2% PVA
Ball penetration depth (mm)	7.3	7.5	8.1
Conductivity of electrolyte ( $\text{mS}\cdot\text{cm}^{-1}$ ) *	$60.10 \pm 0.10$	$59.93 \pm 0.25$	$61.46 \pm 0.21$
1st gelling time	4 h	6 h	11 h
2nd gelling time (after disturbance)	1.5 h	2.2 h	3.1 h

\* Conductivity of the conventional aqueous electrolyte:  $63.16 \pm 1.30 (\text{mS}\cdot\text{cm}^{-1})$ .

The conductivity values of the pristine aqueous electrolyte containing 2M  $\text{Li}_2\text{SO}_4$  and 1M  $\text{ZnSO}_4$  with the pH value of  $4.00 \pm 0.05$ , and its gel form with 5% FS were  $63.16 \pm 1.30 \text{ mS}\cdot\text{cm}^{-1}$  and  $60.10 \pm 0.10 \text{ mS}\cdot\text{cm}^{-1}$ , respectively. These are the two most basic electrolytes, from which we have developed various gels by improving the gelling time, reducing the corrosion, etc. For example, the 5% FS gel was modified by corrosion inhibitors or other gelling agents. Several of these have been published previously. A drop of conductivity value of about 5% is expected since the fume silica is electrochemically inert. Partial replacement of the fumed silica by polyvinyl alcohol does not change the conductivity very much. The 4% FS + 1% PVA gel exhibits  $59.93 \pm 0.25 \text{ mS}\cdot\text{cm}^{-1}$ , and the 4% FS + 1% PVA gel exhibits  $61.46 \pm 0.21 \text{ mS}\cdot\text{cm}^{-1}$ . These values are at the same magnitude of the conductivity of the sulphuric acid electrolytes of lead-acid batteries, and they are about two orders of magnitude higher than conventional non-aqueous electrolytes for Li-ion batteries (e.g., one hundred  $\text{mS}\cdot\text{cm}^{-1}$  vs. several  $\text{mS}\cdot\text{cm}^{-1}$ ). High ionic conductivity is beneficial in establishing a good secondary battery possessing high rate capability and/or high area loading of cathode/anode materials. In our case, the gels are successfully prepared without sacrificing too much conductivity. The ball penetration depth and the gelling time increase vs. the concentration of PVA. In general, our gels have just slightly longer formation periods than the gels used in valve-regulated lead-acid batteries, but

both are in the preferred range of a few hours. This is because fumed silica is used up to 8–12 wt% in the gel electrolytes of lead acid batteries [24]. We only use 3–5 wt% of fumed silica and ensure a sufficient gelling duration so that the electrolyte can be dispersed into AGM separators. The gel electrolyte possessing more than 5 wt% of fumed silica was not adopted because gelation occurred in less than a minute and it was not able to push the gel into the AGM separator. The combination of the AGM and gel electrolyte is always favoured in industry because this gives sufficient performance at low fabrication cost and very low maintenance cost [28].

The FTIR spectra of the PVA, fumed silica (FS), and the three gel electrolytes are reported in Figure S1. On the FTIR spectrum of FS, peaks at  $1070\text{ cm}^{-1}$  and  $799\text{--}807\text{ cm}^{-1}$  are attributed to the asymmetric stretching and the symmetric stretching of Si–O–Si, respectively. On the FTIR spectrum of PVA, the peak at  $3289\text{ cm}^{-1}$  is for –O–H stretching; this wave number is slightly reduced due to the existence of hydrogen bonding. The peak  $2912\text{ cm}^{-1}$  is from the C–H stretching of C–H bond in the methylene group. The  $1722\text{ cm}^{-1}$  peak is for the carbonyl stretching and  $1086\text{ cm}^{-1}$  is for C–O–C vibration. The peak  $840\text{ cm}^{-1}$  is for  $\text{CH}_2$  rocking or C–CH<sub>3</sub> stretching vibration modes. In three gel electrolytes, –O–H vibrational bands at  $3252\text{--}3263\text{ cm}^{-1}$ ,  $1640\text{--}1643\text{ cm}^{-1}$ , and  $607\text{--}612\text{ cm}^{-1}$  are significantly high due to the existence of water and surface silanol groups on the silica materials [29–31]. The peak at  $607\text{--}612\text{ cm}^{-1}$  represents the defect structure of the gel [31]. Hydrogen bonding plays a vital role in gel formation and the stabilisation of the whole system.

Using a three-electrode setup, some electrochemical properties at equilibrium and dynamic states can be revealed. Through linear polarisation (potentiodynamic polarisation) and Tafel fit against the obtained data, we obtained the equilibrium potential and the corrosion current density (after normalising the current to the current per  $\text{cm}^2$ ) on the surface of the zinc working electrode when in contact with different electrolytes (Figure 1). The presence of PVA clearly has a positive role in suppressing corrosion since the corrosion current density is statistically decreased with the increase in the PVA concentration. Under a dynamic condition where the electrodeposition of zinc is enforced by applying a fixed overpotential of 120 mV, the response from each electrolyte is unique (Figure 2). In the case of using a Newtonian liquid electrolyte, the surface area of the zinc working electrode increases, and thus, the absolute value of the responded chronoamperometric current keeps increasing. This is certainly the behaviour of dendritic deposition, and we can see more evidence from the microscopy result (Figure 3a). In case of using gel electrolytes, the chronoamperometric current response and the zinc growth exhibit another kind of behaviour. The current drops were sharp within the first few seconds, then all recovered to similar values (Table 2). Further microscopy investigation provides some more details. Figure 3b shows the SEM of post-run zinc electrode after being immersed in the 5% FS electrolyte. It is flat in most space. This is the desired type of deposition, and it would be ideal if corrosion is not too severe. Partially replacement of the fumed silica by hydrophilic polymers could lengthen the gelling duration, but the polymer could facilitate or reduce side reactions on the zinc electrode. We certainly need to decrease corrosion, passivation, and dendrite formation. So, the gel formulation with PVA offers one-of-a-kind gel electrolyte with multiple advantages: low corrosion, non-dendritic or very low dendritic deposition (with proper concentration), and adjustable gelling time and gel strength, without the need to use any additive. The deposition product from the 4% FS + 1% PVA is very dense on a large scale (Figure 3c—noting that the magnification of this image is lower than others to give a better view), while the deposition product from the 3% FS + 2% PVA is flake-like, with porosity. This suggests that higher concentration of PVA is not favourable, as the deposition from the corresponding gel may not form dense and flat zinc deposits.

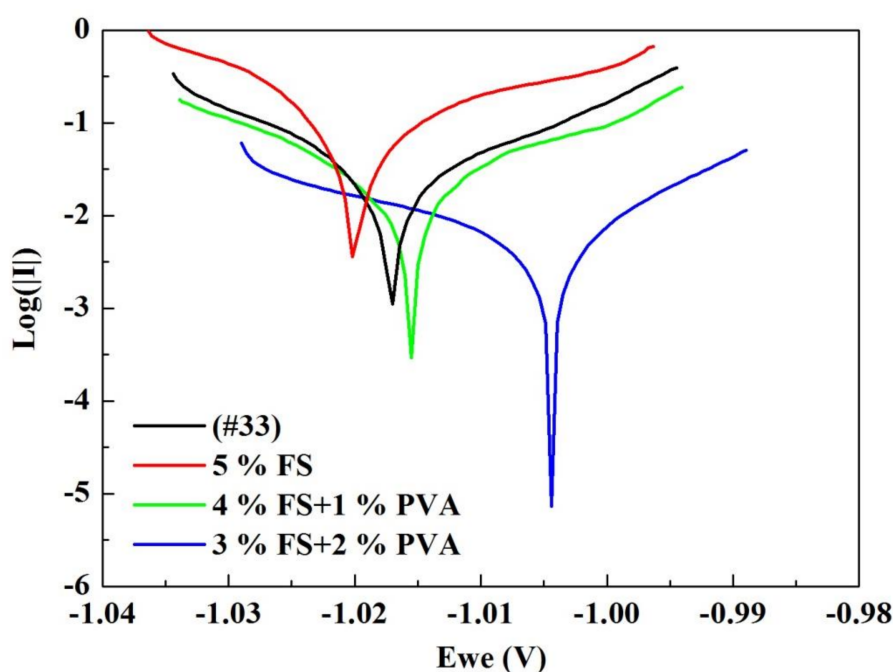


**Figure 1.** Linear polarisation observed when the zinc working electrode is in contact with different electrolytes.

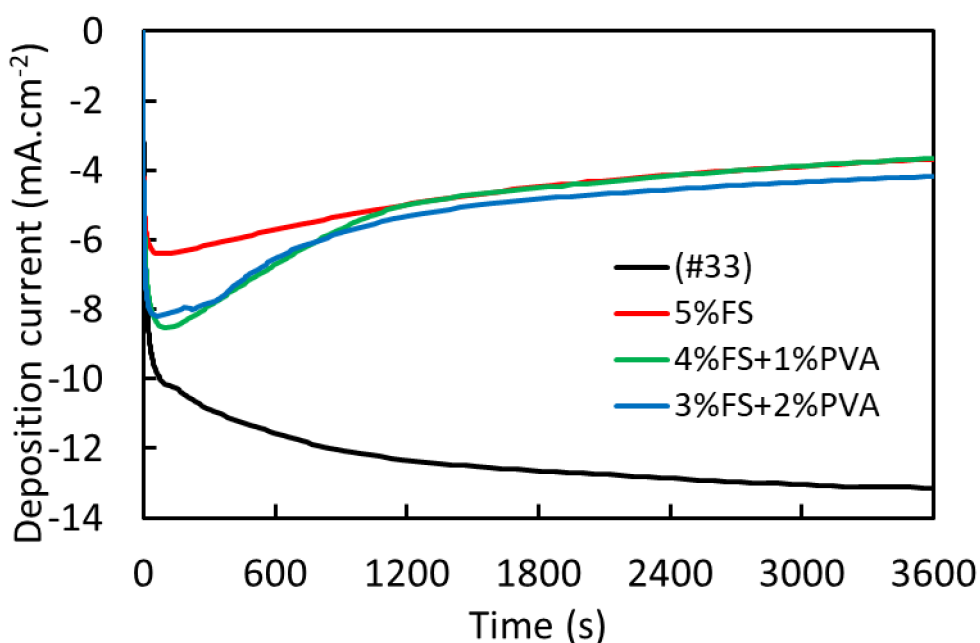


**Figure 2.** Chronoamperometric current density response observed on the zinc electrode when in contact with different electrolytes.

The batteries assembled from  $\text{LiMn}_2\text{O}_4$  cathode, polished zinc foil anode, and different electrolytes were studied with different tests, including cyclic voltammetry (CV), rate capability, open-circuit voltage monitoring (OCV), float charging, cycling under different conditions (constant current, constant current constant voltage, usage of Swagelok, and coin cell). Results are summarised in Table 3, Figures 4, 5 and S2–S5 (Supporting Information). First, the CVs resemble the characteristics of  $\text{LiMn}_2\text{O}_4$  in the testing voltage window with some variations in the position and intensity of peaks. On the first set of redox peaks in between 1.75–1.85 V vs.  $\text{Zn}^{2+}/\text{Zn}$ , the batteries using PVA containing gel electrolytes offer deliver almost identical responses to the battery using aqueous electrolyte, indicating the

immobilisation of water molecules in the quasi-solid gel does not affect the first step of Li<sup>+</sup> extraction/insertion of LiMn<sub>2</sub>O<sub>4</sub>. On the later redox pair, the reference battery shows the highest peak intensity while the 5% FS shows the lowest. Even the difference is small, it reflects a slightly negative effect of the 5% FS gel on the polarisation of the battery and the Li<sup>+</sup> extraction/insertion. Adding PVA results in the slight improvement of peak intensity and reduction in polarisation.

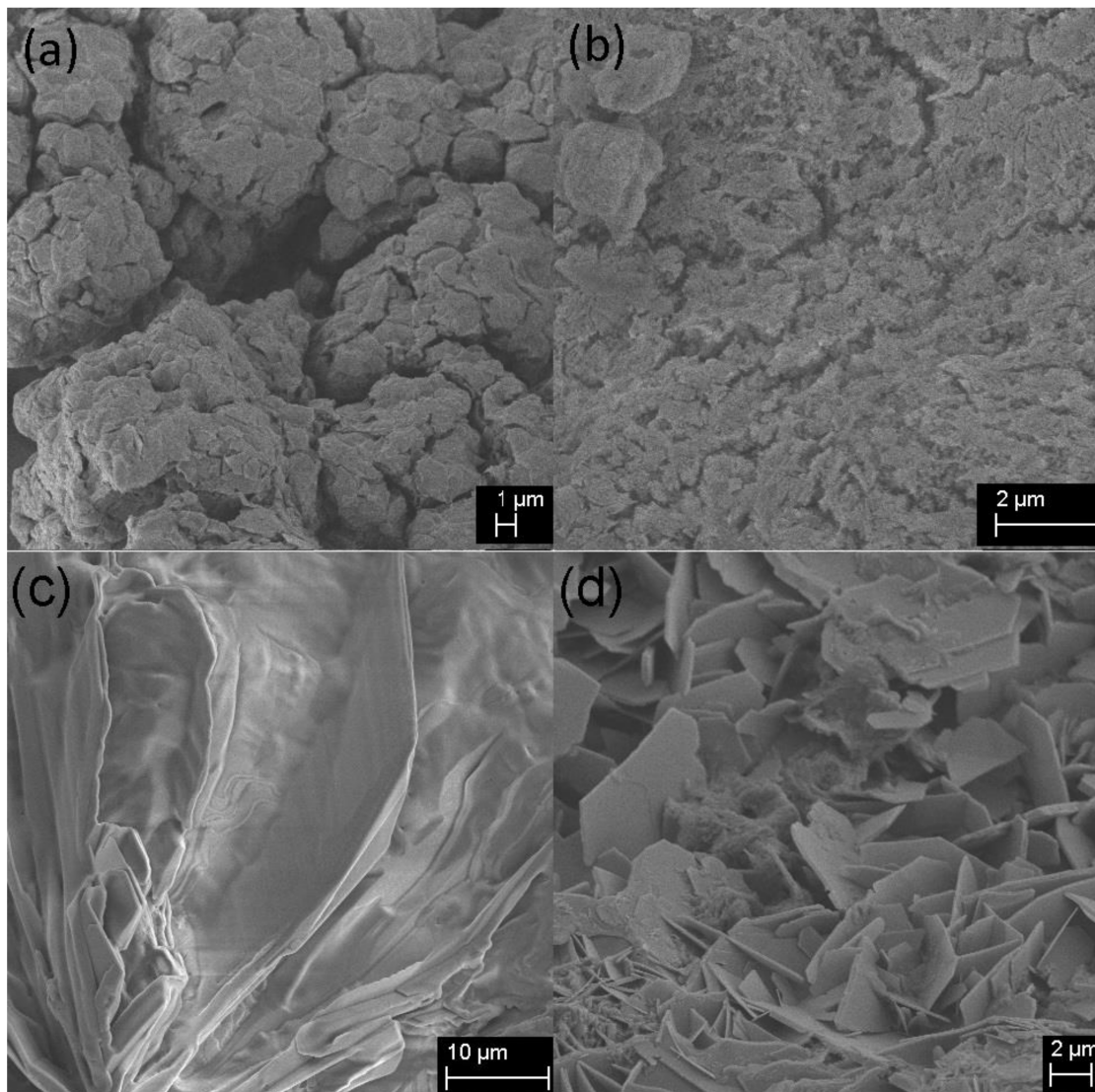


**Figure 3.** SEM of the zinc working electrode after the chronoamperometry experiment. (a) from electrolyte (#33), (b) from 5% FS, (c) from 4% FS + 1% PVA, and (d) from 3% FS + 2% PVA electrolyte.

**Table 2.** Corrosion potential, corrosion current density, and chronoamperometry current density of the zinc working electrode in contact with different electrolytes.

Type of Electrolyte	Corrosion Potential (mV)	Corrosion Current Density ( $\mu\text{A}\cdot\text{cm}^{-2}$ )	Chronoamperometry Current Density ( $\text{mA}\cdot\text{cm}^{-2}$ )
(#33)	$-1016.32 \pm 1.07$	$5.25 \pm 0.57$	$-13.1438$
5% FS	$-1019.93 \pm 0.10$	$19.73 \pm 2.34$	$-3.6809$
4% FS + 1% PVA	$-1015.87 \pm 0.46$	$5.7922 \pm 1.13$	$-3.6542$
3% FS + 2% PVA	$-1003.84 \pm 0.24$	$1.4096 \pm 0.82$	$-4.1765$

**Table 3.** Rate capability ( $\text{mAh} \cdot \text{g}^{-1}$ ), float current ( $\text{mA} \cdot \text{cm}^{-2}$ ), and open-circuit voltage (V) of the conventional (ref) and gel batteries.

Battery	1st Discharge 0.2 C	1st Discharge 4 C	1st Discharge 0.2 C <sup>a</sup>	Float Current <sup>b</sup>	Open Circuit Voltage <sup>c</sup>
The conventional	$120.02 \pm 3.83$	$95.59 \pm 7.01$	$118.48 \pm 5.08$	$0.008 \pm 0.001$	$1.947 \pm 0.014$
5% FS	$121.14 \pm 2.99$	$97.54 \pm 1.98$	$119.72 \pm 1.91$	$0.0067 \pm 0.00058$	$1.970 \pm 0.005$
4% FS + 1% PVA	$134.25 \pm 4.41$	$109.63 \pm 7.20$	$129.96 \pm 4.79$	$0.01 \pm 0.0014$	$1.956 \pm 0.009$
3% FS + 2% PVA	$133.67 \pm 7.13$	$106.97 \pm 9.04$	$128.45 \pm 4.87$	$0.01067 \pm 0.0015$	$1.968 \pm 0.012$

<sup>a</sup> After 5 cycles at 0.2 C, 5 cycles at 0.5 C, 5 cycles at 1 C, 5 cycles at 2 C, and 5 cycles at 4 C. <sup>b,c</sup> after 24 h of monitoring.

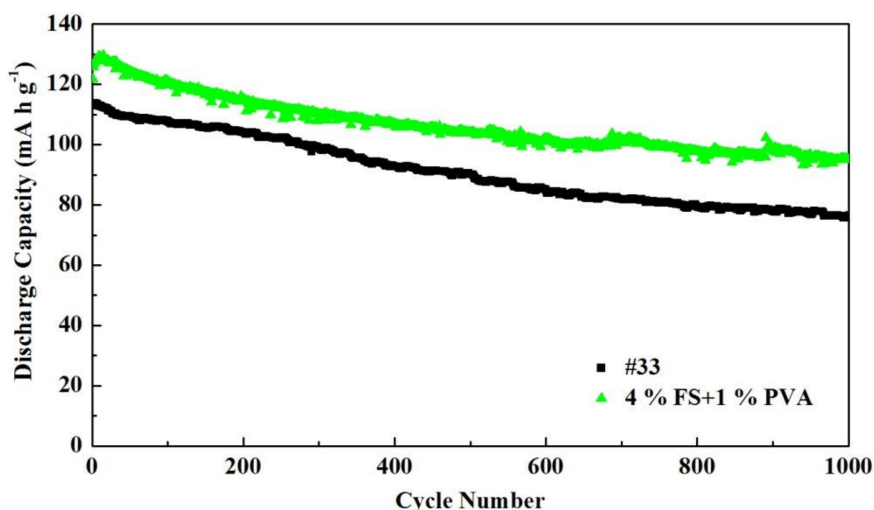


**Figure 4.** Cyclability of the 4% FS + 1% PVA and the reference coin cell.

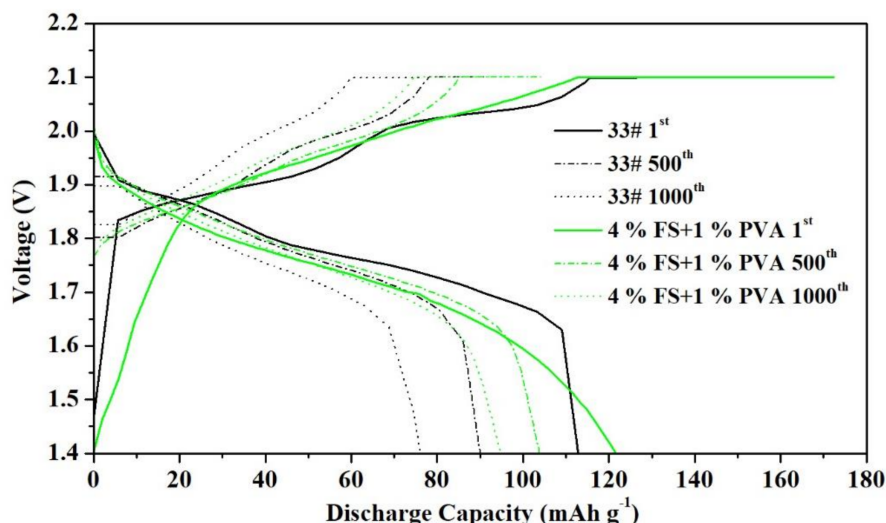


**Figure 5.** Voltage profile of the reference and the gel battery at 1st, 500th, and 1000th cycles.

Figure S3 and the final column in Table 2 represent the open-circuit voltage of the batteries after continuous monitoring for 24 h. This test started after the batteries were charged to 2.1 V using CC-CV mode. It is known that the initial voltage drops during OCV monitoring for all kinds of secondary aqueous batteries (Li-ion, zinc-ion, NiMH, lead-acid ...) are much larger than non-aqueous batteries, and it was revealed that gelled batteries generally exhibit higher resistance toward self-discharge under monitoring during the first few hours [32–35]. However, the float charge current density does not decrease in batteries using the PVA-FS gels but slightly on those using the 5% FS. This could be

explained using corrosion data in conjunction with the chronoamperometry results plus corresponding microscopy results. During float charging, the zinc ions are forced to reduce, followed by the deposition on the anode, while the corrosion dissolves the zinc back to the electrolyte as zinc ions. More corrosion means the current (or the capacity) spent on float charging is higher to help the battery maintain its full state of charge. The corrosion current density observed on the Zn electrode when in contact with 4% FS + 1% PVA is still as high as  $5.7922 \pm 1.13 \mu\text{A}\cdot\text{cm}^{-2}$ . The 3% FS + 2% PVA presents much lower corrosion current density. However, the highly porous flake-like deposit (Figure 3d) leads to the increase in the surface area of the zinc electrode, which will enhance the total corrosion on this electrode in the long run because corrosion depends on the surface area.

The existence of PVA in the gels improves the specific discharge capacity of the Zn/LiMn<sub>2</sub>O<sub>4</sub> battery by 10–12%, especially at low C-rate (e.g., C/5) (Table 3 and Figure 4). This may be due to the better wettability or adhesion at the interface [36,37]. It is known that PVA containing gel electrolytes are being exploited in Li-ion pseudo-capacitors and supercapacitors because the PVA is robust toward fast Li<sup>+</sup> ion transport, as well as maintaining the functionality of the cathode–electrolyte interface [38,39]. At higher rate (e.g., 4 C), the capacities of batteries using PVA containing electrolytes are still high, but the error bar is also larger. Additionally, the battery with the 3% FS + 2% PVA electrolyte seems to have a more serious fluctuation even though it presents low corrosion current density, indicating that it may not be reasonable to increase the concentration of PVA in the electrolyte to higher than 2 wt%.

Figures S4 and S5 (Supporting Information) show the cycling results up to 1000 cycles, under CC mode (Figure S4) and CC-CV mode (Figure S5). The CC-CV mode increases the capacity retention, so the results from Figure S5 are generally higher than that in Figure S4. However, similar features between these two modes can be observed. First, the reference battery using aqueous electrolyte works well in first few hundred cycles; even the difference may be considered small. After that, however, the best gelled battery starts to take the lead in all setups and all cycling conditions. This is due to the rapid deterioration of both the cathode and the anode in aqueous electrolyte, which can be clearly seen on the XRD of the post-run cathode (Figure S6) and anode (Figure S7) and the microscopy results (Figure S8). On Figure S6, all patterns are normalised by using the peak (111); the other peaks of LiMn<sub>2</sub>O<sub>4</sub> are generally lower on the post-run cathode of the reference battery, reflecting some degrees of amorphization of the LiMn<sub>2</sub>O<sub>4</sub> surface. This phenomenon is not clearly observed in other samples. It is worthy to point out that the intensity of the peaks of the zinc electrode from the post-run reference battery are the lowest. However, with the increase in the PVA concentration, the XRD peaks become broader, which suggests the depositions of non-conducting materials on the anode due to passivation and supports the conclusion that there is a critical point of the PVA concentration in the electrolyte for improving the battery performance. This passivation issue can be further confirmed by the SEM on Figure S8g, which shows some degree of local charging due to the less-conducting surface. Thus, it is understandable why the capacity retention of this 3% FS + 2% PVA battery is not as good as other batteries in the series.

Figures 4, 5 and S9 represent the cyclability of the best gelled coin cell and the reference coin cell. It is obvious that the coin cell results are much smoother than the Swagelok cell. The capacity delivered by the gelled coin cell is always higher than the reference, and it can retain about 100 mAh·g<sup>-1</sup> capacity, even after 1000 cycles. This is the best result to date for gelled Zn/LiMn<sub>2</sub>O<sub>4</sub> batteries, and it is undoubtedly a promising system to apply in the scaling-up process. Figure 5 provides the CC-CV charge–discharge curves for the reference (#33) and the 4% FS + 1% PVA batteries at the 1st, 500th, and 1000th cycles. At the beginning, the gelled battery needs more energy to be fully charged. The distance between the charge–discharge curve is larger than that of the reference. However, this distance shrinks to one smaller than that of the reference after about 500 cycles. This may be due to the more severe amorphization on the cathode of the reference, and other side reactions. On the other hand, the gelled battery is much more stable once it gets through a

conditioning period. This agrees with other physical and electrochemical characterisations presented in previous parts.

#### 4. Conclusions

A simple non-Newtonian electrolyte system has been designed for the Zn/LiMn<sub>2</sub>O<sub>4</sub> battery. Only one thixotropic and one non-thixotropic gelling agent are required to formulate with the pristine aqueous electrolyte. Through physical, mechanical, and electrochemical studies, the necessary properties of the gel electrolytes are revealed, including the gel strength, gelling duration, and conductivity. FTIR reveals that hydrogen bonding plays a key role during gel formation and self-healing of the gels after mechanical disturbance. The corrosion current density on the zinc electrode is available for all kinds of electrolytes, and they are in the range of few  $\mu\text{A}\cdot\text{cm}^{-2}$ . The chronoamperometry plus ex situ microscopy confirms the non-dendritic or dendritic zinc deposition from the electrolyte. Such properties are used to explain the battery performance via C-rate studies, float charge, self-discharge, and cyclability. The best gelled battery stands out with exceptional cyclability ( $\sim 100 \text{ mAh}\cdot\text{g}^{-1}$  capacity after 1000 cycles and nearly 80% retention), 6–10% higher discharge capacity, and better rate capability versus the reference battery. Self-discharge is also reduced. We also point out that assembly methods affect the battery performance. Ex situ crystallography and microscopy of post-run electrodes reveal less amorphization of cathode materials and less passivation on the anode surface when using appropriate gel electrolytes in the Zn/LiMn<sub>2</sub>O<sub>4</sub> battery.

**Supplementary Materials:** The following supporting information can be downloaded at: <https://www.mdpi.com/article/10.3390/batteries8070071/s1>, Figure S1: FTIR of PVA, FS, 3%FS+2%PVA, 4%FS+1%PVA, and 5%FS gel electrolytes; Figure S2: CV of the conventional Swagelok battery using the aqueous electrolyte (33), and batteries using 5%FS, 4%FS+1%PVA, and 3%FS+2%PVA gel electrolytes; Figure S3: Open circuit voltage monitoring of typical conventional Swagelok battery, and batteries using 5%FS, 4%FS+1%PVA, and 3%FS+2%PVA gel electrolytes; Figure S4: Cycle at 4C, constant current mode cycling of typical conventional Swagelok battery, and batteries using 5%FS, 4%FS+1%PVA, and 3%FS+2%PVA gel electrolytes; Figure S5: Cycle 4C, constant current – constant voltage cycling of typical conventional Swagelok battery, and batteries using 5%FS, 4%FS+1%PVA, and 3%FS+2%PVA gel electrolytes. The current cut-off during constant voltage charge at 2.1V is 10% of the charging current at 4C; Figure S6: XRD patterns of the post-cycling cathodes of typical conventional Swagelok battery, and batteries using 5%FS, 4%FS+1%PVA, and 3%FS+2%PVA gel electrolytes. The batteries were cycled under standard constant current mode at 4C; Figure S7: XRD patterns of the post-cycling anodes of typical conventional Swagelok battery, and batteries using 5%FS, 4%FS+1%PVA, and 3%FS+2%PVA gel electrolytes. The batteries were cycled under standard constant current mode at 4C; Figure S8: SEM images of the post-cycling anodes and cathodes of typical conventional Swagelok battery (a and b), and batteries using 5%FS (c and d), 4%FS+1%PVA (e and f), and 3%FS+2%PVA (g and h) gel electrolytes. The batteries were cycled under standard constant current mode at 4C; Figure S9: Coulombic efficiencies of the reference and gelled battery.

**Author Contributions:** Conceptualization, P.C. and T.K.A.H.; methodology, J.Z.; experiment and data curation, T.K.A.H., L.L., J.Z., T.N.L.D. and W.D.; X.H., Y.X., J.M. and M.C.; writing—original draft preparation, T.K.A.H.; writing—review and editing, P.C.; supervision, P.C.; project administration, P.C.; funding acquisition, P.C. and T.K.A.H. All authors have read and agreed to the published version of the manuscript.

**Funding:** This research was funded by Mitacs (IT61045), The University of Waterloo, and Positec Group Ltd.

**Institutional Review Board Statement:** Not applicable.

**Informed Consent Statement:** Not applicable.

**Data Availability Statement:** All data are presented in the manuscript and in the Supporting Information for publication. Further sharing or discussion of data for the purpose of reproducing this work is available upon reasonable request.

**Conflicts of Interest:** The authors declare no conflict of interest.

## References

1. Liu, H.; Wang, J.-G.; You, Z.; Wei, C.; Kang, F.Y.; Wei, B. Rechargeable aqueous zinc-ion batteries: Mechanism, design strategies and future perspectives. *Mater. Today* **2021**, *42*, 73–98. [[CrossRef](#)]
2. Hollax, E. Advanced electrochemical energy sources for space power system—A review. *J. Power Sources* **1979**, *4*, 11–19. [[CrossRef](#)]
3. Borchers, N.; Clark, S.; Horstmann, B.; Jayasayee, K.; Juel, M.; Stevens, P. Innovative zinc-based batteries. *J. Power Sources* **2021**, *484*, 229309. [[CrossRef](#)]
4. Kordesh, K.; Weissenbacher, M. Rechargeable alkaline manganese dioxide/zinc batteries. *J. Power Sources* **1994**, *51*, 61–78. [[CrossRef](#)]
5. Liu, Q.; Pan, Z.; Wang, E.; An, L.; Sun, G. Aqueous metal-air batteries: Fundamentals and applications. *Energy Storage Mater.* **2020**, *27*, 478–505. [[CrossRef](#)]
6. Dubarry, M.; Qin, N.; Brooker, P. Calendar aging of commercial Li-ion cells of different chemistries—A review. *Curr. Opin. Electrochem.* **2018**, *9*, 106–133. [[CrossRef](#)]
7. Gao, Y.; Zhang, X.; Cheng, Q.; Guo, B.; Yang, J. Classification and review of the charging strategies for commercial lithium-ion batteries. *IEEE Access* **2019**, *7*, 43511–43524. [[CrossRef](#)]
8. Battistel, A.; Palagonia, M.S.; Brogioli, D.; la Mantia, F.; Trócoli, R. Electrochemical Methods for Lithium Recovery: A Comprehensive and Critical Review. *Adv. Mater.* **2020**, *32*, 1905440. [[CrossRef](#)]
9. Pereira, A.; Paoletta, A.; Dubé, J.; Champagne, D.; Mauger, A.; Zaghib, K. State of charge influence on thermal reactions and abuse tests in commercial lithium-ion cells. *J. Power Sources* **2018**, *399*, 392–397. [[CrossRef](#)]
10. Zhang, H.; Li, C.; Eshetu, G.G.; Laruelle, S.; Grugueon, S.; Zaghib, K.; Julien, C.; Mauger, A.; Guyomard, D.; Rojo, T.; et al. From Solid-Solution Electrodes and the Rocking-Chair Concept to Today’s Batteries. *Angew. Chem. Int. Ed.* **2020**, *59*, 534–538. [[CrossRef](#)]
11. Chen, S.; Lan, R.; Humphreys, J.; Tao, S. Perchlorate Based “Oversaturated Gel Electrolyte” for an Aqueous Rechargeable Hybrid Zn–Li Battery. *ACS Appl. Energy Mater.* **2020**, *3*, 2526–2536. [[CrossRef](#)]
12. Xu, Z.; Fan, Q.; Li, Y.; Wang, J.; Lund, P.D. Review of zinc dendrite formation in zinc bromine redox flow battery. *Renew. Sustain. Energy Rev.* **2020**, *127*, 109838. [[CrossRef](#)]
13. Cai, Z.; Ou, Y.; Wang, J.; Xiao, R.; Fu, L.; Yuan, Z.; Zhan, R.; Sun, Y. Chemically resistant Cu–Zn/Zn composite anode for long cycling aqueous batteries. *Energy Storage Mater.* **2020**, *27*, 205–211. [[CrossRef](#)]
14. Olbasa, B.W.; Fenta, F.W.; Chiu, S.-F.; Tsai, M.-C.; Huang, C.-J.; Jote, B.A.; Beyene, T.T.; Liao, Y.-F.; Wang, C.-H.; Su, W.-N.; et al. High-Rate and Long-Cycle Stability with a Dendrite-Free Zinc Anode in an Aqueous Zn-Ion Battery Using Concentrated Electrolytes. *ACS Appl. Energy Mater.* **2020**, *3*, 4499–4508. [[CrossRef](#)]
15. Zampardi, G.; Compton, R.G. Fast electrodeposition of zinc onto single zinc nanoparticles. *J. Solid State Electrochem.* **2020**, *24*, 2695–2702. [[CrossRef](#)] [[PubMed](#)]
16. Clark, S.; Borchers, N.; Jusys, Z.; Behm, R.J.; Horstmann, B. Aqueous Zinc Batteries. In *Encyclopedia of Electrochemistry*; John Wiley & Sons: Hoboken, NJ, USA, 2020. Available online: <https://onlinelibrary.wiley.com/doi/10.1002/9783527610426.bard110022> (accessed on 12 July 2022).
17. Hoang, T.K.A.; Doan, T.N.L.; Sun, K.E.K.; Chen, P. Corrosion chemistry and protection of zinc & zinc alloys by polymer-containing materials for potential use in rechargeable aqueous batteries. *RSC Adv.* **2015**, *5*, 41677–41691.
18. Gaberšček, M.; Pejovnik, S. Impedance spectroscopy as a technique for studying the spontaneous passivation of metals in electrolytes. *Electrochim. Acta* **1996**, *41*, 1137–1142. [[CrossRef](#)]
19. Shen, X.-W.; Li, Y.-T.; Qian, T.; Liu, J.; Zhou, J.-Q.; Yan, C.-L.; Goodenough, J.B. Lithium anode stable in air for low-cost fabrication of a dendrite-free lithium battery. *Nat. Commun.* **2019**, *10*, 900. [[CrossRef](#)]
20. Lu, W.; Xie, C.; Zhang, H.; Li, X. Inhibition of Zinc Dendrite Growth in Zinc-Based Batteries. *ChemSusChem* **2018**, *11*, 3996–4006. [[CrossRef](#)]
21. Mainar, A.R.; Colmenares, L.C.; Blazquez, J.A.; Urdampilleta, I. A brief overview of secondary zinc anode development: The key of improving zinc-based energy storage systems. *Int. J. Energy Res.* **2018**, *42*, 903–918. [[CrossRef](#)]
22. Yadav, P.K.; Raghav, S.; Raghav, J.; Swarupa Tripathy, S.S. Electrolytes for Zn-Ion Batteries. In *Zinc Batteries: Basics, Developments, and Application*; Boddula, R., Inamuddin Asiri, A.M., Eds.; Scrivener Publishing & Wiley and Sons: Hoboken, NJ, USA, 2020; pp. 51–72.
23. Beck, F.; Ruetschi, P. Rechargeable batteries with aqueous electrolytes. *J. Power Sources* **2000**, *45*, 2467–2482. [[CrossRef](#)]
24. Lambert, D.W.H.; Greenwood, P.H.J.; Reed, M.C. Advances in gelled-electrolyte technology for valve-regulated lead-acid batteries. *J. Power Sources* **2002**, *107*, 173–179. [[CrossRef](#)]
25. Hoang, T.K.A.; Doan, T.N.L.; Cho, J.H.; Su, J.Y.J.; Lee, C.; Lu, C.; Chen, P. Sustainable Gel Electrolyte Containing Pyrazole as Corrosion Inhibitor and Dendrite Suppressor for Aqueous Zn/LiMn<sub>2</sub>O<sub>4</sub> Battery. *Chemsuschem* **2017**, *10*, 2816–2822. [[CrossRef](#)] [[PubMed](#)]
26. Tantchanakul, T.; Chailapakul, O.; Tantavichet, N. Influence of Fumed Silica and Additives on the Gel Formation and Performance of Gel Valve-regulated Lead-acid Batteries. *J. Ind. Eng. Chem.* **2013**, *19*, 2085–2091. [[CrossRef](#)]
27. Pan, K.; Shi, G.; Li, A.; Li, H.; Zhao, R.; Wang, F.; Zhang, W.; Chen, Q.; Chen, H.; Xiong, Z.; et al. The Performance of a Silica-based Mixed Gel Electrolyte in Lead Acid Batteries. *J. Power Sources* **2012**, *209*, 262–268. [[CrossRef](#)]

28. Tonazzzo, V. The key to success: Gelled-electrolyte and optimized separators for stationery lead-acid batteries. *J. Power Sources* **2006**, *158*, 1124–1132. [[CrossRef](#)]
29. Losq, C.L.; Cody, G.D.; Mysen, B.O. Complex IR spectra of OH<sup>-</sup> groups in silicate glasses: Implications for the use of the 4500 cm<sup>-1</sup> IR peak as a marker of OH<sup>-</sup> groups concentration. *Am. Mineral.* **2015**, *100*, 945–950. [[CrossRef](#)]
30. Dingemans, G.; van Helvoirt, C.A.A.; Pierreux, D.; Keuning, W.; Kessels, W.M.M. Plasma-Assisted ALD for the Conformal Deposition of SiO<sub>2</sub>: Process, Material and Electronic Properties. *J. Electrochem. Soc.* **2012**, *159*, H277. [[CrossRef](#)]
31. Bertoluzza, A.; Fagnano, C.; Morrelli, M.A.; Gottardi, V.; Guglielmi, M. Raman and infrared spectra on silica gel evolving toward glass. *J. Non-Cryst. Solids* **1982**, *48*, 117–128. [[CrossRef](#)]
32. User Manual of Seabird Nickel Metal Hydride Battery. Available online: [https://web.archive.org/web/20090227062546/http://www.seabird.com/pdf\\_documents/manuals/NiMH\\_002.pdf](https://web.archive.org/web/20090227062546/http://www.seabird.com/pdf_documents/manuals/NiMH_002.pdf) (accessed on 7 May 2019).
33. Catherino, H.A.; Shi, P.; Rusek, A.; Feres, F. Self-Discharging of Lead-Acid Batteries. *SAE Tech. Pap. Ser.* **2000**, *1*, 0305.
34. Cui, J.; Wu, X.; Yang, S.; Li, C.; Tang, F.; Chen, J.; Chen, Y.; Xiang, Y.; Wu, X.; He, Z. Cryptomelane-Type KMn<sub>8</sub>O<sub>16</sub> as Potential Cathode Material—For Aqueous Zinc Ion Battery. *Front. Chem.* **2018**, *6*, 352. [[CrossRef](#)] [[PubMed](#)]
35. Suo, L.; Borodin, O.; Sun, W.; Fan, X.; Yang, C.; Wang, F.; Gao, T.; Ma, Z.; Schroeder, M.; von Cresce, A.; et al. Advanced High-Voltage Aqueous Lithium-Ion Battery Enabled by “Water-in-Bisalt” Electrolyte. *Angew. Chem. Int. Ed.* **2016**, *55*, 7136–7141. [[CrossRef](#)] [[PubMed](#)]
36. Zhu, Y.S.; Wang, X.J.; Hou, Y.Y.; Gao, X.W.; Liu, L.L.; Wu, Y.P.; Shimizu, M. A new single-ion polymer electrolyte based on polyvinyl alcohol for lithium ion batteries. *Electrochim. Acta* **2013**, *87*, 113–118. [[CrossRef](#)]
37. Amaral, F.A.; Dalmolin, C.; Canobre, S.C.; Bocchihttps, N.; Rocha-Filho, R.C.; Biaggio, S.R. Electrochemical and physical properties of poly(acrylonitrile)/poly(vinyl acetate)-based gel electrolytes for lithium ion batteries. *J. Power Sources* **2007**, *164*, 379–385. [[CrossRef](#)]
38. Wang, G.; Lu, X.; Ling, Y.; Zhai, T.; Wang, H.; Tong, Y.; Li, Y. LiCl/PVA gel electrolyte stabilizes vanadium oxide nanowire electrodes for pseudocapacitors. *ACS Nano* **2012**, *6*, 10296–10302. [[CrossRef](#)]
39. Zhang, X.; Wang, L.; Peng, J.; Cao, P.; Cai, X.; Li, J.; Zhai, M. A Flexible Ionic Liquid Gelled PVA-Li<sub>2</sub>SO<sub>4</sub> Polymer Electrolyte for Semi-Solid-State Supercapacitors. *Adv. Mater. Interfaces* **2015**, *12*, 1500267. [[CrossRef](#)]